Contents

Chapter 3

Scientific Goals

3.1 Introduction

The primary goal of the GlueX project is the definitive and detailed mapping of the spectrum of a new family of particles called *hybrid mesons*. Linearly polarized photons produced by electrons from an energy-upgraded CEBAF will be the probe used to uncover this spectrum. This experimental information is absolutely critical in finding the answer to an outstanding and fundamental questions in physics – a quantitative understanding of the confinement mechanism in quantum chromodynamics.

The spectrum of mesons and baryons uncovered during the 1960's led to the quark model within which mesons are bound states of a quark and antiquark, $q\bar{q}$, and baryons are bound states of three quarks, qqq. Further experimental work indicated that quarks are dynamical objects as well and this led to the development of quantum chromodynamics (QCD), the theory of quarks and gluons and their interactions modeled after the very successful theory of quantum electrodynamics (QED). Just as charged particles interact by the exchange of photons, quarks, with their color charge, interact by exchanging gluons. There are however important and fundamental differences between the two theories. There are three types of color charge as opposed to one kind of electrical charge. And the gluons of QCD also carry color charge and can interact with quarks and each other. In contrast, the photons of QED do not carry charge. Bound states involving quarks and gluons or qluons alone are thus possible and indeed should exist. QCD also incorporates the experimental fact that the quarks and gluons do not exist as free particles by requiring that only color singlet combinations exist as free particles in nature. In addition to the color singlet combinations $q\bar{q}$ and qqq others are possible, such as $q\bar{q}g$ (*hy-*

brid mesons) and gg or ggg (*glueballs*). These new states, collectively known as *gluonic excitations*, are fascinating since this is the only case of a theory in which the gauge particle is also a constituent. The analogous states in QED, like atoms of light, cannot exist. Although there is tantalizing evidence for these gluonic excitations, their spectra have not been mapped out.

The confinement of quarks and gluons within the particles of which they are the constituents is a unique feature of QCD. But a quantitative understanding of the confinement mechanism still eludes us. Theoretical progress is being made and lattice QCD, based on first-principle calculations, will ultimately be able to predict a detailed spectrum, including masses and decays, of hybrid mesons and glueballs. The experimental information about the spectrum of this new form of matter as predicted by QCD is an essential ingredient for the ultimate understanding of the confinement mechanism.

The low-lying glueball states will be searched for in the glue-rich J/ψ radiative decays as part of the planned CLEO-c project at Cornell's CESR. However the low-lying glueballs posses J^{PC} quantum numbers that are the same as $q\bar{q}$ states and therefore mixing with conventional $q\bar{q}$ mesons is possible and that can complicate glueball identification. In contrast, hybrid mesons can possess J^{PC} quantum numbers not possible for $q\bar{q}$. These *exotic hybrid mesons* thus have a *smoking gun signature*. Just as nonets of $q\bar{q}$ mesons made of the three light quarks (u, d and s) exist, nature should also reveal nonets of hybrids with the same flavor quantum numbers but with now with the possibility of exotic J^{PC}. Hybrid mesons should also have widths comparable to conventional mesons. This is supported by theoretical considerations and by the possible sighting of an exotic hybrid in π^--induced interactions.

Hybrid mesons can be thought of as $q\bar{q}g$ bound states in which the gluon is a constituent. An attractive alternative picture is one in which a gluonic flux tube forms between the q and $\bar{q}$ in a meson. This flux tube forms because of the self-interaction of the gluons and qualitatively accounts for confinement. It leads to a linear potential, or a force that is constant as the distance between the quark and anti-quark varies. Infinite energy is required to separate the quarks to infinity, thus qualitatively accounting for confinement. This notion of a relativistic string or flux tube between the quarks was introduced in the 1970's to account for the observed linear dependence of particle mass-squared (m^2) on spin (J). The flux tube concept is supported by lattice QCD studies. Within this picture conventional mesons result when the flux tube is in its ground state. Hybrid mesons arise when the flux tube is excited. The lack of information on this spectroscopy is due in part to the complicated decay modes favored by these states. Another is due to the apparent suppression of exotic hybrid mesons in production mechanisms with π or K probes. On

the other hand production of exotic hybrid mesons is expected to be favored using beams of photons and essentially no data exist on the photoproduction of light mesons. The GLUEX project will remedy this situation.

In addition to providing for a linearly polarized photon beam of sufficient energy, the GLUEX project includes construction of a hermetic detector to allow for particle identification and momentum and energy determination sufficient to allow for complete kinematic reconstruction of events with a wide variety of final states. This is essential for the spin analysis – partial wave analysis (PWA) – needed to determine the J^{PC} quantum numbers, to map out the flavor quantum numbers of the hybrid nonets and to test assumptions about the details of confinement that would lead to predicting specific decay modes.

In this chapter we expand on the following:

1. *Spectroscopy of Light Mesons.* This will include a brief review of the conventional quark model and the status of the light quark meson spectrum.

2. *Gluonic excitations and the role in QCD.* This will include a discussion of how the gluons form flux tubes, and how their excitations lead to QCD mesons, in particular exotic hybrids. This general picture is not restricted to a particular model but follows from the first-principles QCD calculations.

3. *The current evidence for gluonic excitations.* The evidence comes from overpopulation of conventional nonets and from possible glueball and exotic hybrid sightings in $\bar{p}p$ annihilations and π-induced interactions.

4. *Photons are expected to be particularly effective in producing exotic hybrids.* Its spin structure makes the photon a qualitatively different probe from π and K beams. The first excited transverse modes of the flux tube can lead to exotic hybrids only when the quark spins are aligned. This argument is consistent with expectations from models based on phenomenological analysis of existing data that predict cross sections for photoproduction of exotic hybrids comparable to those of normal mesons. And there are essentially no data on photoproduction of light mesons so this is *terra incognita*. The existing photoproduction data will be discussed.

5. *The complementarity of this study with other planned projects that will study gluonic excitations.* We will compare this to searches in the charm

quark or beauty quark sectors or e^+e^- annihilations, in particular the GSI Project and the CLEO-c Project at Cornell.

6. *The importance of the PWA technique in uncovering exotic mesons.* The PWA is a powerful analysis tool that has been successfully employed in experiments to uncover states which are not evident from a simple examination of mass spectra (bump-hunting). PWA is absolutely essential for this project as is the development of the formalism for incident photon beams and an understanding of the phenomenology. The importance of a hermetic detector with excellent resolution and rate capability and sensitivity to a wide variety of decay modes will be discussed.

7. *Linear polarization of the photon beam is essential for this study.* Linear polarization is important in the determination of the J^{PC} quantum numbers and it is essential in determining the production mechanism. Linear polarization can be used as a filter for exotics once the production mechanism is isolated.

8. *The ideal photon energy range.* In order to reach the desired mass range we need to be far enough above threshold so that the decay products of produced mesons can be detected and measured with sufficient precision. High enough energies are also important to avoid line-shape distortions of higher-mass mesons. We also want to be high enough in energy to kinematically separate production of baryon resonances from production of meson resonances. This need for higher energies, however is balanced by a need for sufficiently low energy to allow for a solenoid-only-based detector to momentum analyze the highest energy charged particles with sufficient accuracy. These considerations lead to an ideal photon energy in the range from 8 to 9 GeV.

9. *The desired electron energy.* Having established the desired photon beam energy of 9 GeV an electron energy must be sufficiently high compared to the desired photon beam energy to achieve a sufficient degree of linear polarization. With 12 GeV electrons, the degree of linear polarization is 40%. If the electron energy drops to 10 GeV the degree of polarization drops to 5%. The ratio of tagged hadronic rate to total hadronic rate in the detector drops as the electron energy approaches the desired photon energy. The conclusion is that an electron energy of 12 GeV suffices but lower energies will severely compromise the physics goals.

3.2 Conventional light mesons

The early version of the quark model described the observed mesons as bound states of a quark and antiquark, where the quarks were assumed to be the u, d and s quarks. Thus mesons were grouped in families with nine members – a nonet – characterized by a given J^{PC} determined by the relative spin of the two quarks and their relative orbital angular momentum. Within the nonet three are members of an isotriplet with zero strangeness. Two are members of an isodoublet with positive strangeness and another two with negative strangeness. And the remaining two members have zero strangeness and isospin. This flavor pattern holds for all the nonets. Radial excitations are also allowed.

The rules for allowed values of J^{PC} follow from the requirements of a fermion–antifermion system: the quark spins can be parallel ($S = 1$) or antiparallel ($S = 0$) with relative orbital angular momentum (L), $\vec{J} = \vec{L} + \vec{S}$, $P = (-1)^{L+1}$ and $C = (-1)^{L+S}$. Thus the low-lying nonet with $\vec{L} = 0$ and $\vec{S} = 0$ leads to $J^{PC} = 0^{-+}$, the pseudoscalar nonet, including the π, K, η and η' mesons. The nonet with $\vec{L} = 0$ and $\vec{S} = 1$ leads to $J^{PC} = 1^{--}$, the vector mesons, including the ρ, K^*, ω and ϕ mesons. The combination $\vec{L} = 1$ and $\vec{S} = 1$ leads to three nonets: scalar ($J^{PC} = 0^{++}$), axial vector ($J^{PC} = 1^{++}$) and tensor ($J^{PC} = 2^{++}$).

Using the rules for determining J^{PC} for a fermion-antifermion system, certain J^{PC} combinations are not allowed for $q\bar{q}$ systems and these include $J^{PC} = 0^{--}$, 0^{+-}, 1^{-+}, 2^{+-}, $\cdots$. Such combinations are referred to as *exotic* quantum numbers. Indeed, that such combinations were not initially observed gave credence to the quark model.

Figure 3.1 shows our current knowledge of conventional $q\bar{q}$ states. The exact association of an observed meson with a particular $q\bar{q}$ state within a nonet depends on a good understanding of the various decay modes of the meson as well as its mass, width and production characteristics. Figure 3.1 also shows the expected range of masses for glueballs, hybrid mesons and meson-meson molecular states. These will be described in more detail below.

The range of masses of the known conventional meson nonets and their radial excitations extend from the π mass up to about 2.5 GeV/c^2. Figure 3.2 shows the spectrum of $q\bar{q}$ states in more detail including radial excitations. There is also now clear evidence that the observed meson spectrum includes states which cannot be accommodated within the naive quark model. For example, there are at least five scalar states reported with masses below 2 GeV/c^2. These, along with indications of exotic J^{PC} sightings will be discussed below.

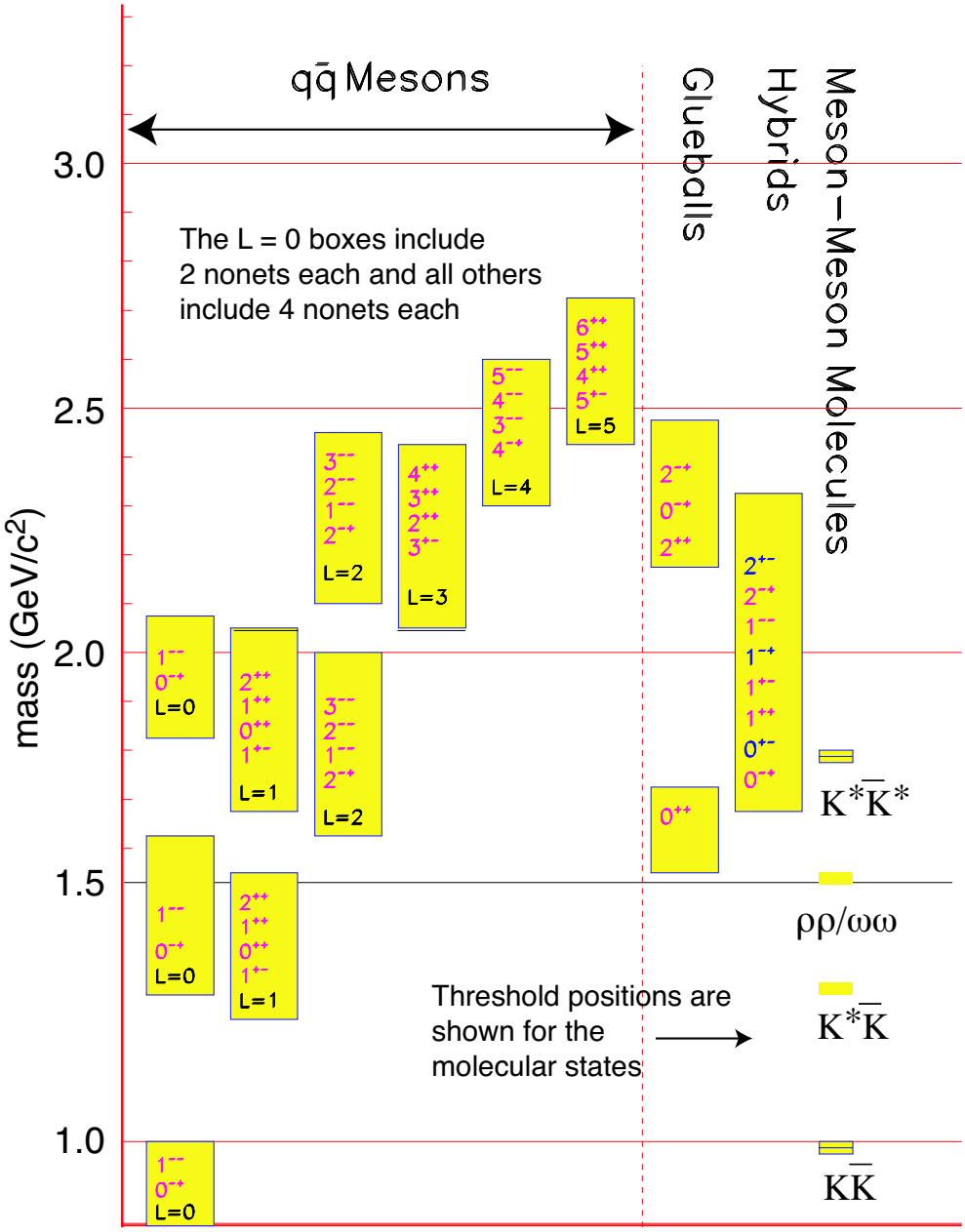

Figure 3.1: A level diagram showing conventional nonets and expected masses of glueballs, hybrids and molecular thresholds. The vertical axis is in units of GeV/c^2. For the $q\bar{q}$ boxes the L refers to the angular momentum between the quarks and each J^{PC} refers to a nonet of mesons. Note also that exotic J^{PC}, – 0^{+-}, 1^{-+}, 2^{+-} – occur only among the hybrids for the range of masses shown.

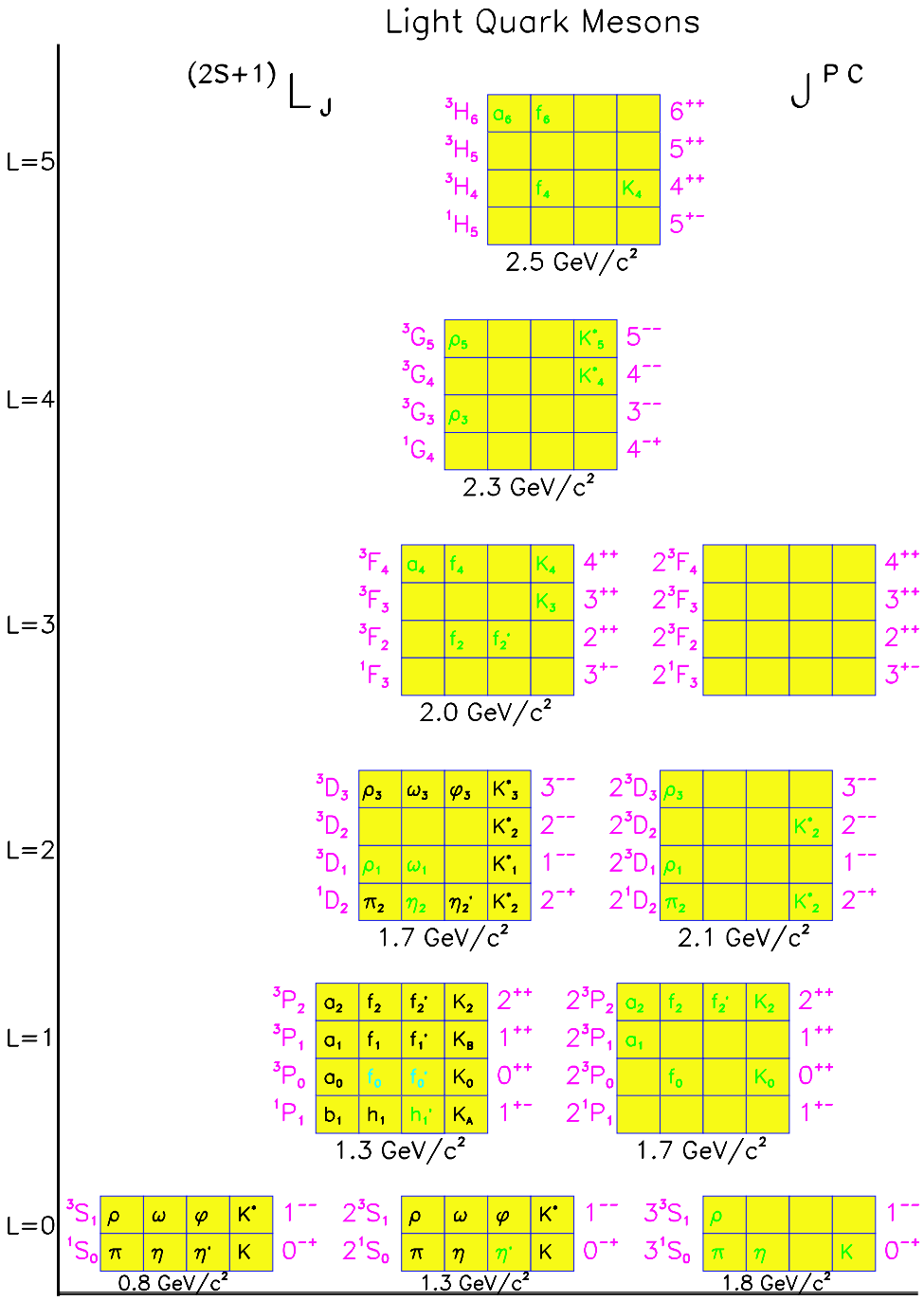

Figure 3.2: The $q\bar{q}$ spectrum of states. The assignments of the light colored states are speculative, while the empty boxes are missing states. The orbital angular momentum of the nonet is plotted on the vertical axis, while the towers of radial excitations are shown along the horizontal axis.

3.3 Gluonic excitations and confinement

The Standard Model of elementary particles includes electroweak theory and QCD, the latter describing the strong interactions among the quarks and gluons. At short distances – the regime of asymptotic freedom – perturbative techniques are applicable and QCD describes high energy experimental phenomena and data both qualitatively and quantitatively. At large distance scales – the confinement regime – the situation is far different. Here the successful calculational techniques of the perturbative regime cannot be used. We must rely on first-principles lattice QCD calculations or QCD-inspired models. There has been significant theoretical effort in this area recently and more progress can be expected in the near future, especially as multi-teraflop lattice QCD centers come into operation.

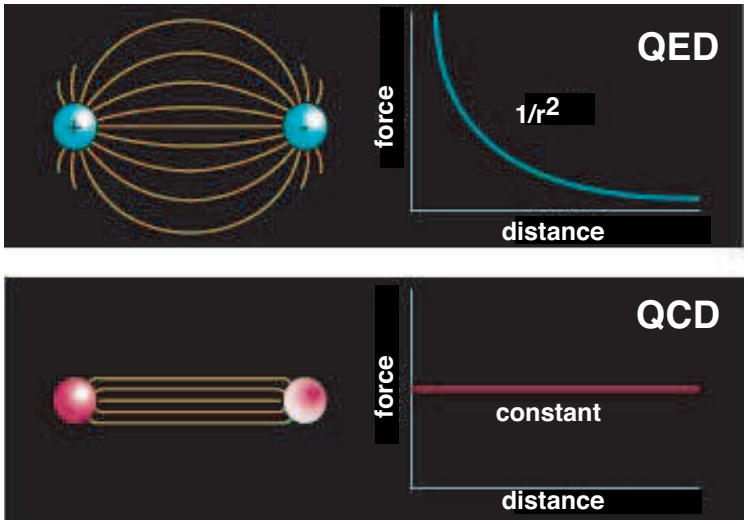

Figure 3.3: Field lines associated with the electrical force between two electrically charged particles (top) and the corresponding dependence of force on the distance between the charges and the field lines associated with the color force (bottom) between two quarks and the corresponding dependence of force on distance.

Understanding confinement in QCD requires a detailed understanding of the role of gluons. QCD is distinct from QED in that the force carriers of the former (gluons) carry color charge whereas for the latter the photons are electrically neutral. As illustrated in Figure 3.3, the force between two electrically charged particles falls off like the inverse square of the distance between the

charges. The number of field lines intersecting a unit area midway between the charges and perpendicular to the line connecting them would decrease as the inverse square of the distance between the charges. In contrast, the color field lines between a quark and an anti-quark do not fill all of space as in the case with electrical charges. Rather the field lines form flux tubes. A unit area placed midway between the quarks and perpendicular to the line connecting them intercepts a constant number of field lines, independent of the distance between the quarks. This leads to a constant force between the quarks – and a large force at that, equal to about 16 metric tons. The potential associated with this constant force is linear and grows with increasing distance. It takes infinite energy to separate the quarks to infinity and thus, qualitatively at least, this accounts for confinement.

Lattice QCD calculations support this notion of the formation of a flux tube between the quark and anti-quark. Figure 3.4 shows the energy density in the color field between a quark and an anti-quark in a meson with a separation of 1.2 $fermi$. The density peaks at the positions of the quarks and is confined to a tube between the quarks. This calculation is for heavy quarks in the quenched approximation. Figure 3.4 also shows the corresponding potential between the quarks. The ground state potential has a $1/r$ dependence at small distances and is linear for large distances.

This notion of the formation of flux tubes was first introduced in the 1970's by Yoichiro Nambu [1] to explain the observed linear Regge trajectories – the linear dependence of mass squared, m^2, of hadrons on their spin, J. This linear dependence results if one assumes that massless quarks are tied to the ends of a relativistic string with constant mass (energy) per length with the system rotating about its center. The linear m^2 versus J dependence only arises when the mass density per length is constant, which is equivalent to a linear potential.

Within this picture, conventional mesons arise when the flux tube is in its ground state. Excitations of the flux tube lead to hybrid mesons that exhibit both the quark and gluonic degrees of freedom. The first excited state of the flux tube is a transverse excitation. The flux tube, or string, spins clockwise or counter-clockwise around the $q\bar{q}$ line leading to two degenerate states – degenerate since the energy should not depend on which way the flux tube is spinning. Lattice QCD and flux tube models both indicate that the lowest excited flux tube has $J = 1$ [2, 3, 4]. The linear combinations of the clockwise or counter-clockwise rotations are eigenstates of parity and charge conjugation leading to two possibilities for the excited flux tube: $J^{PC} = 1^{-+}$ or $J^{PC} = 1^{+-}$. Suppose we start with the $q\bar{q}$ in the $S = 0$ and $L = 0$ (or $J^{PC} = 0^{-+}$ – the π or K) configuration. Combining this with $J^{PC} = 1^{-+}$ or $J^{PC} = 1^{+-}$ of the

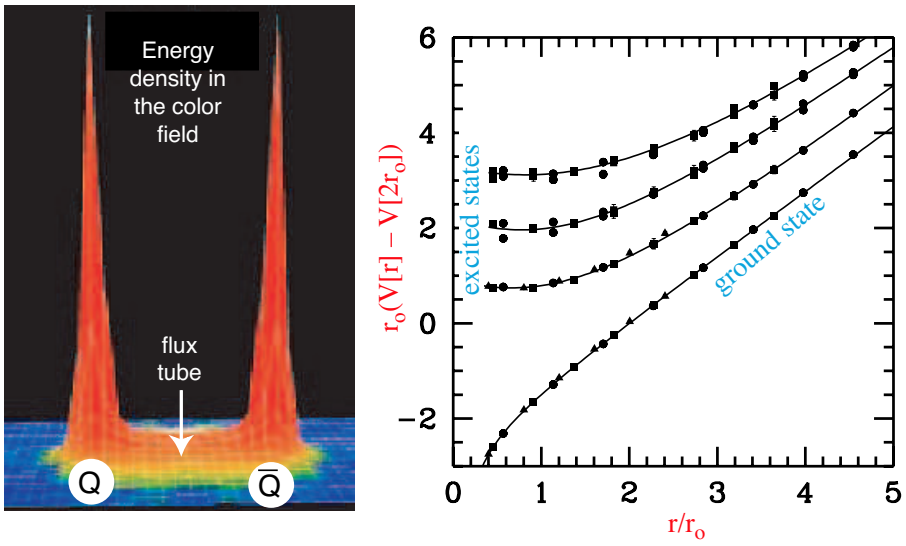

Figure 3.4: (left) A lattice QCD calculation of the energy density in the color field between a quark and an anti-quark. The density peaks at the positions of the quarks and is confined to a tube between the quarks. This calculation is for heavy quarks in the quenched approximation. (right) The corresponding potential between the quarks. The ground state potential has a $1/r$ dependence at small distances and is linear for large distances.

excited flux tube results in hybrid mesons with $J^{PC} = 1^{++}$ or $J^{PC} = 1^{--}$. These are non-exotic quantum numbers. If, however, we start with $q\bar{q}$ in the $S = 1$ and $L = 0$ (or $J^{PC} = 1^{--}$ – the vector photon) configuration, the resulting hybrid meson can have $J^{PC} = [0, 1, 2]^{+-}$ for the flux tube with $J^{PC} = 1^{-+}$ and $J^{PC} = [0, 1, 2]^{-+}$ for the flux tube with $J^{PC} = 1^{+-}$. We note that of these six possible J^{PC} combinations, three are exotic: $J^{PC} = 0^{+-}$, $J^{PC} = 1^{-+}$ and $J^{PC} = 2^{+-}$. These states will not mix with $q\bar{q}$ and thus have unique signatures.

Meson production proceeds with an an incoming probe interacting with the target particle and one result of the scattering can be the excitation of the flux tube. If the probe is a $q\bar{q}$ in $L = 0$ and $S = 0$ (π or K), production of exotic hybrids will not be favored. But if the $q\bar{q}$ probe has $L = 0$ and $S = 1$, for example a photon, one expects exotic hybrids to be produced readily.

Finally we consider the expected masses for hybrid mesons. We would expect the mass difference between the ground state (conventional) mesons and hybrid mesons to be given by the level spacing between the ground state of the flux tube and the first excited transverse mode and that is simply given by π/r where r is the quark separation. When translated to appropriate units this corresponds to about 1 GeV/c^2.

In this discussion the motion of the quarks was ignored, but we know from general principles [5] that an approximation that ignores the impact of the flux tube excitation and quark motion on each other seems to work quite well.

3.4 Observation of gluonic excitations

3.4.1 Glueballs

Lattice QCD calculations indicate that lightest glueball is a scalar with a mass in the range from 1.5 to 1.7 GeV/c^2 [6, 7, 8, 9]. Indeed there is evidence from the Crystal Barrel experiment, which studied $\bar{p}p$ annihilations at CERN, that the $f_0(1500)$ is a leading candidate for a glueball [10, 11]. There are, however, indications that this state is not a pure glueball but is mixed with conventional $q\bar{q}$ [12]. There are also strong indications that the scalar meson sector contains one or more glueballs since there are several more observed states than can be accommodated in the simple $q\bar{q}$ model. However, the unique identification of a glueball is exacerbated by the possibility of mixing with $q\bar{q}$. Lattice QCD indicates a rich spectrum of glueballs, all with non-exotic quantum numbers, from 1.5 to 2.5 GeV/c^2. The lightest glueball with exotic quantum numbers is predicted to have $J^{PC} = 2^{+-}$ and to have a mass of 4 GeV/c^2 [6].

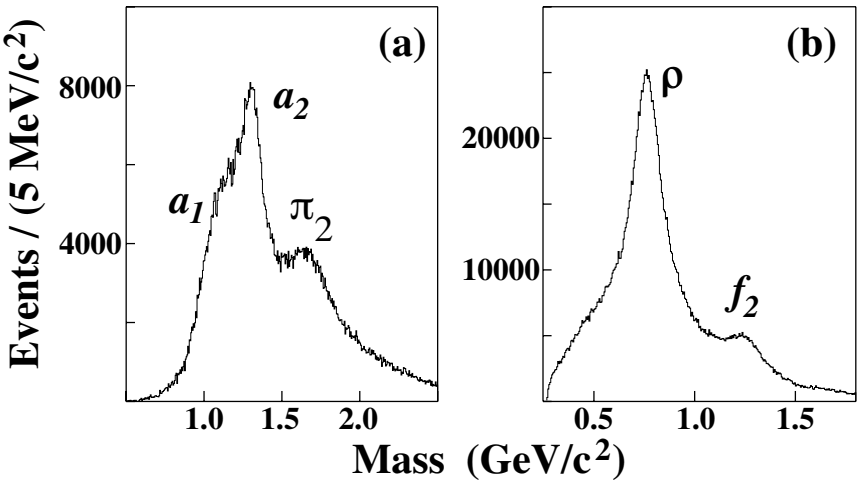

Figure 3.5: Acceptance corrected effective mass distributions for the (a) $\pi^+\pi^-\pi^-$ combination and (b) $\pi^+\pi^-$ combination (two entries per event) from E852 [13].

3.4.2 Exotic hybrid mesons

After about two decades of experimental searches there have been reports of experimental observations of states with exotic $J^{PC} = 1^{-+}$ by the Brookhaven E852 collaboration in $\pi^- p$ interactions at 18 GeV/c. One of these has a mass of $(1593 \pm 8^{+29}_{-47})$ MeV/c^2 and width of $(168 \pm 20^{+150}_{-12})$ MeV/c^2 and decays into $\rho^0\pi^-$ [13].

This state was observed in the reaction $\pi^- p \to \pi^+\pi^-\pi^- p$ at a beam momentum of 18 GeV/c. In Figure 3.5, the acceptance-corrected (average acceptance was 25%) distributions of the $\pi^+\pi^-\pi^-$ and $\pi^+\pi^-$ effective masses are shown. The positions of well-established meson states are shown, including the $a_1(1260)$, which does not show up as a prominent peak in the overall mass distribution. The partial wave analysis (PWA) performed on these data assumes an *isobar model* – a parent decaying into a $\pi\pi$ state and an unpaired π followed by the decay of the $\pi\pi$ state. The resulting decomposition into various waves is shown in Figure 3.6. The decomposition clearly shows the $\pi(1800)$ in the 0^{-+} wave, the $a_1(1260)$ in the 1^{++} wave, the $\pi_2(1670)$ in the 2^{-+} wave, and the $a_2(1320)$ in the 2^{++} wave. Evidence for the exotic 1^{-+} $\rho\pi$ is shown in Figure 3.7. If an isovector $\rho\pi$ resonates in an $L = 1$ wave, it has $J^{PC} = 1^{-+}$. Also shown in this figure is the effect of leakage of non-exotic waves. Finally in Figure 3.8 a coupled fit to the wave intensities and phase difference between the 1^{-+} and 2^{-+} waves is shown.

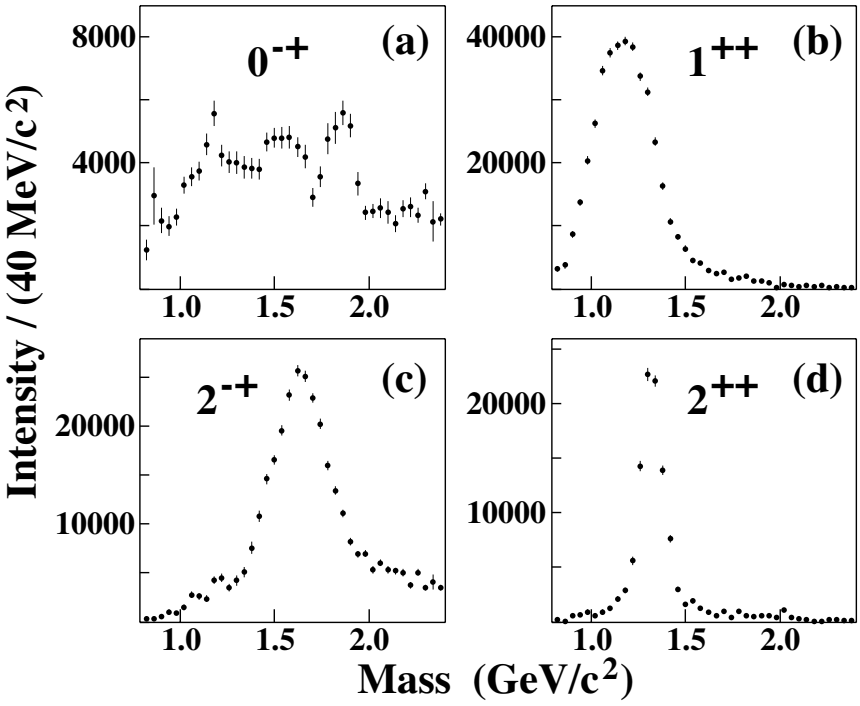

Figure 3.6: Combined intensities for all (a) 0^{-+} waves; (b) 1^{++} waves; (c) 2^{-+} waves; and (d) 2^{++} waves from E852 [13].

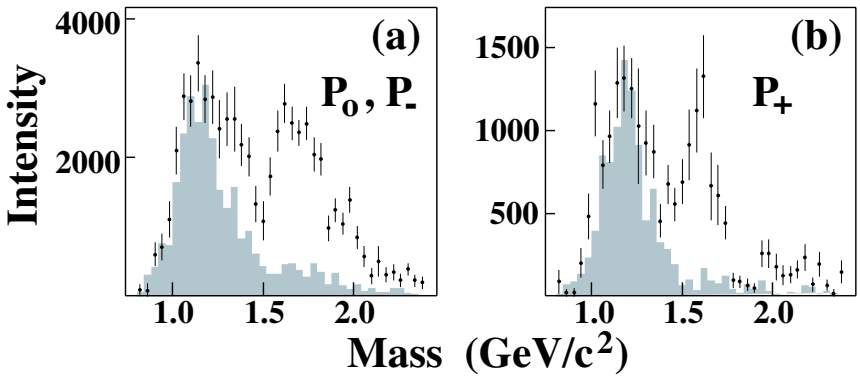

Figure 3.7: The intensities for the waves corresponding to 1^{-+} into $\rho\pi$. The shaded distributions are an estimate of leakage due to non-exotic waves – from E852 [13].

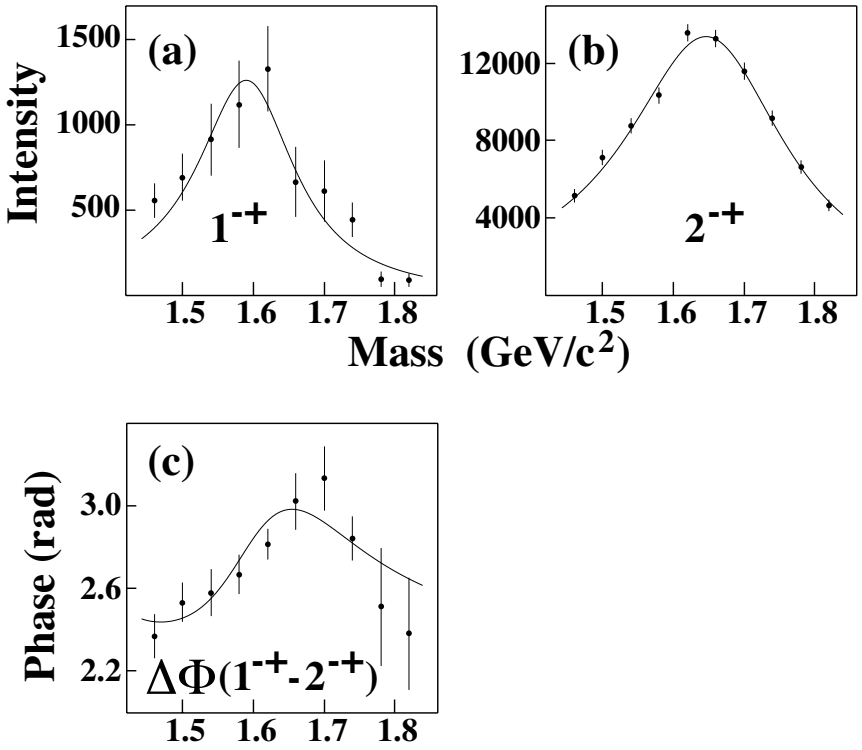

Figure 3.8: Results of a coupled mass-dependent Breit-Wigner fit of the 1^{-+} and 2^{-+} waves showing the phase difference as well – from E852 [13].

Another state reported by E852 has a similar mass, $(1597 \pm 10^{+45}_{-10})\ MeV/c^2$, but with a significantly larger width,$(340 \pm 40^{+50}_{-50})\ MeV/c^2$, and decays into $\eta'\pi^-$ [14]. It has not been determined whether these represent two decay modes of the same state or whether they are due to two different mechanisms.

The E852 collaboration also reported observation of another $J^{PC} = 1^{-+}$ state with mass $(1370 \pm 16^{+50}_{-30})\ MeV/c^2$ and a width of $(385 \pm 40^{+65}_{-105})\ MeV/c^2$ decaying into $\eta\pi^-$ [15]. If an $\eta\pi$ system is in a P wave, the resulting J^{PC} quantum number combination is exotic (1^{-+}). In these studies the dominant state observed in the $\eta\pi$ channel is the $J^{PC} = 2^{++}$ $a_2(1320)$ seen in the D-wave. Critical to the identification of this state is not only showing the presence of a P-wave, but also that the resulting line shape is consistent with a Breit-Wigner and that the phase motion of the P, as determined by its interference with the dominant D-wave, cannot be due solely to the $a_2^-(1320)$ resonance. Soon after the E852 report, the Crystal Barrel Collaboration reported an exotic $J^{PC} = 1^{-+}$ state produced in $\bar{p}n \to \pi^-\pi^0\eta$ obtained by stopping antiprotons in liquid deuterium [16]. They reported a mass of $(1400 \pm 20^{+20}_{-20})\ MeV/c^2$ and a width of $(310 \pm 50^{+50}_{-30})\ MeV/c^2$.

The first claim of an exotic meson decaying into $\eta\pi^0$ with a mass of 1400 MeV/c^2 was made by the GAMS collaboration in the reaction $\pi^-p \to \eta\pi^0 n$ [17] but a later analysis by the group [18] led to ambiguous results. The VES collaboration also presented evidence for a P-wave contribution in $\eta\pi$ [19] and at KEK a claim was made for an exotic $\eta\pi$ state [20] as well, but with a mass and width close to that of the $a_2(1320)$; leakage from the dominant D wave could not be excluded.

In all the observations in π-induced reactions, the $\eta\pi$ P-wave enhancements have cross sections that are substantially smaller than the dominant $a_2(1320)$ so this leakage, usually due to an imperfect understanding of experimental acceptance, is a source of concern. In contrast, the observed yield of the $\pi_1(1400)$ yield in $\bar{p}p$ annihilations is of the same magnitude as the $a_2(1320)$. Apart from these experimental issues, the interpretation of the nature of low-mass $\eta\pi$ P-wave amplitude and phase motion should be guided by the principle of parsimony – less exotic interpretations must also be considered. In a recent analysis of the $\eta\pi^0$ system in the reaction $\pi^-p \to \eta\pi^0 n$ from data using the E852 apparatus, a P-wave is observed but it is not consistent with a Breit-Wigner resonance. The observed P-wave phase motion is consistent with $\eta\pi^0$ final state interactions. This could explain the relatively wide width of the observed $\eta\pi^-$ state and could also explain the broad $\eta'\pi^-$ enhancement. The $\pi^-p \to \eta\pi^0 n$ and $\pi^-p \to \eta\pi^- p$ have some notably differences. For the former charge conjugation (C) is a good quantum number but not for the latter and for the former both the $a_0(980)$ and $a_2(1320)$ are prominently present but for

the latter only the $a_2(1320)$ is strongly produced. This is an important factor in selecting the physical solutions among mathematically ambiguous solutions.

The conclusion from these studies is that there indeed are tantalizing hints of gluonic excitations in both the glueball and hybrid sectors but the results are not conclusive. The large statistics samples of high quality data to be collected with the GLUEX detector will provide the definite resolution of the murky situation. Furthermore there is good reason to believe that whereas exotic hybrids may be suppressed in π production, they are enhanced in photoproduction where essentially no data exist. In the glueball sector, the large samples of glue-rich radiative J/ψ decays should shed light on the spectrum of these gluonic excitations.

3.5 Photoproduction of exotic hybrids

3.5.1 Why photoproduction?

Based on the arguments presented above, the photon is expected to be particularly effective in producing the *smoking gun* signature for gluonic excitations: hybrids with exotic J^{PC}. In this regard, we will compare the effectiveness of the π or K as a probe with that of the photon. In the former case, the meson is a $q\bar{q}$ with spins anti-aligned ($S = 0$) and in the latter, the photon is a virtual $q\bar{q}$ with spins aligned ($S = 1$). In both cases, the relative orbital angular momentum is zero ($L = 0$) and the flux tube connecting the quarks is in its ground state. Figure 3.9 illustrates the differences between a π probe and a γ probe. If the scattering results in excitation of the flux tube, one expects exotic hybrid mesons to be suppressed in π-induced interactions and enhanced in photoproduction.

Current phenomenology also supports the notion that photons should be more effective at producing exotic hybrids [21, 22]. Figure 3.10 shows an estimate of the photoproduction cross sections at 8 GeV for the $a_2(1320)$ and the exotic $\pi_1(1600)$ [22]. The model uses as input the ratio of $\pi_1(1600)$ to $a_2(1320)$ as observed in E852. The model is compared with photoproduction of the $a_2(1320)$ at 5 GeV. Whereas in E852, with a π beam, the $\pi_1(1600)$ is produced at about 5% of the rate for $a_2(1320)$, in photoproduction the rates for $\pi_1(1600)$ are expected to be comparable for that of the $a_2(1320)$. In the case of the incident π, the $\pi_1(1600)$ is produced by ρ exchange and the suppression at very low-$|t|$ due to angular momentum – spin 0 in and spin 1 out – decreases the cross section. This is to be compared to photoproduction of the $\pi_1(1600)$ with π exchange where there is no suppression at very low-$|t|$ since now we

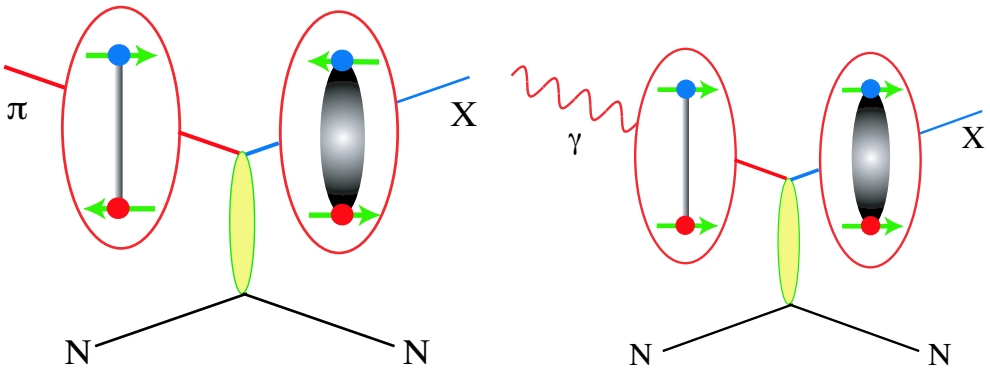

Figure 3.9: (left) With a π probe the incoming quarks have $L = 0$ and $S = 0$. The excited flux tube from the scattering results in hybrid mesons with non-exotic quantum numbers. (right) With a photon probe the incoming quarks have $L = 0$ and $S = 1$. When the flux tube is excited, hybrid mesons with exotic quantum numbers are possible.

have spin 1 in and spin 1 out. Furthermore the $N\rho N$ coupling at the baryon vertex in the incident π case is lower by a factor of 4 compared to the $N\pi N$ in the photoproduction case.

To underscore the differences between existing photoproduction and π production, the corresponding largest data sets on 3π production are compared in the plots of Figure 3.11. The 3π mass spectrum from the reaction $\pi^- p \to \pi^+\pi^-\pi^- p$ at 18 GeV/c from E852 at Brookhaven is shown. Also shown is the 3π mass spectrum from the reaction $\gamma p \to \pi^+\pi^+\pi^- n$ at 19 GeV from SLAC. We note the large difference in statistics between the two and we also note the differences in the structure of the spectra.

3.5.2 Current photoproduction data

Table 3.1 is a partial compilation of known photoproduction cross sections and the numbers of events from the existing experiments. The typical cross sections range from of order 0.1 μb up to of order 10 μb, with most measurements involving rather small numbers of events, typically on the order of a few thousand. The extant data from photoproduction are far too meager to perform the analysis necessary to unambiguously identify gluonic excitations. For example, after one year of low intensity running at 10^7 photons/sec, the yield of $a_2(1320)$ in GlueX will be five orders of magnitude greater than the same collected in the SLAC photoproduction experiment. The yield of the

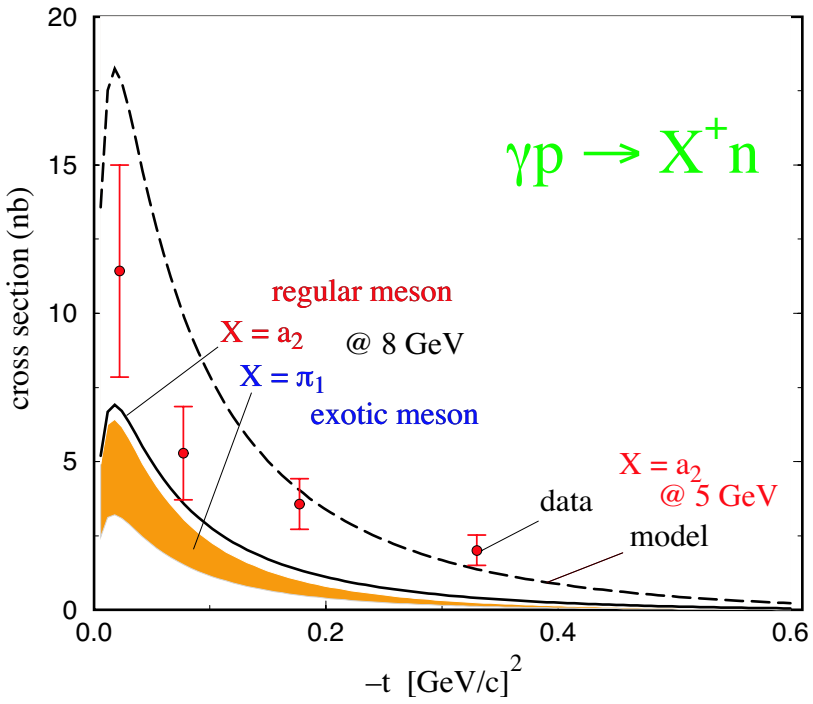

Figure 3.10: Estimates of the photoproduction cross sections for $a_2(1320)$ and the exotic $\pi_1(1600)$ at 8 GeV based on a phenomenological analysis described in [22]. The model uses as input the ratio of $\pi_1(1600)$ to $a_2(1320)$ as observed in E852. The model is compared with photoproduction of the $a_2(1320)$ at 5 GeV.

Reaction	E_γ *GeV*	σ (μb)	*Events*	*Ref.*
$\gamma p \to p\pi^+\pi^-$	9.3		3500	[23]
$\gamma p \to p\pi^+\pi^-$	19.3		20908	[24]
$\gamma p \to p\pi^+\pi^-\pi^\circ$	2.8		2159	[23]
$\gamma p \to p\pi^+\pi^-\pi^\circ$	4.7		1606	[23]
$\gamma p \to p\pi^+\pi^-\pi^\circ$	9.3		1195	[23]
$\gamma p \to p\pi^+\pi^-\pi^\circ$	4.7–5.8	$13.5 \pm 1.5\,\mu b$	3001	[25]
$\gamma p \to p\pi^+\pi^-\pi^\circ$	6.8–8.2	$11.8 \pm 1.2\,\mu b$	7297	[25]
$\gamma p \to n\pi^+\pi^+\pi^-$	4.7–5.8	$4.6 \pm 1.4\,\mu b$	1723	[25]
$\gamma p \to n\pi^+\pi^+\pi^-$	6.8–8.2	$4.0 \pm 1.2\,\mu b$	4401	[25]
$\gamma p \to n\pi^+\pi^+\pi^-$	16.5–20		3781	[26]
$\gamma p \to p\pi^+\pi^-\pi^\circ$	20–70		14236	[27]
$\gamma p \to p\pi^+\pi^-\pi^+\pi^-$	4–6	$4.0 \pm 0.5\,\mu b$	~ 330	[28]
$\gamma p \to p\pi^+\pi^-\pi^+\pi^-$	6–8	$4.8 \pm 0.5\,\mu b$	~ 470	[28]
$\gamma p \to p\pi^+\pi^-\pi^+\pi^-$	8–12	$4.5 \pm 0.6\,\mu b$	~ 470	[28]
$\gamma p \to p\pi^+\pi^-\pi^+\pi^-$	12–18	$4.4 \pm 0.6\,\mu b$	~ 380	[28]
$\gamma p \to p\pi^+\pi^-\pi^+\pi^-$	15–20		6468	[29]
$\gamma p \to p\pi^+\pi^-\pi^\circ\pi^\circ$	20–70		8100	[30]
$\gamma p \to p\pi^+\pi^+\pi^-\pi^-\pi^\circ$	19.5		2553	[31]
$\gamma p \to \Delta^{++}\pi^-\pi^+\pi^-$	4–6	$1.65 \pm 0.2\,\mu b$	~ 200	[28]
$\gamma p \to \Delta^{++}\pi^-\pi^+\pi^-$	6–8	$1.8 \pm 0.2\,\mu b$	~ 200	[28]
$\gamma p \to \Delta^{++}\pi^-\pi^+\pi^-$	8–12	$1.1 \pm 0.2\,\mu b$	~ 200	[28]
$\gamma p \to \Delta^{++}\pi^-\pi^+\pi^-$	12–18	$1.15 \pm 0.2\,\mu b$	~ 200	[28]
$\gamma p \to p\omega$	4.7–5.8	$2.3 \pm 0.4\,\mu b$	< 1600	[25]
$\gamma p \to p\omega$	6.8–8.2	$2.0 \pm 0.3\,\mu b$	< 1200	[25]
$\gamma p \to p\omega$	4.7	$3.0 \pm 0.3\,\mu b$	1354	[23]
$\gamma p \to p\omega$	9.3	$1.9 \pm 0.3\,\mu b$	1377	[23]
$\gamma p \to p\phi$	4.7	$0.41 \pm 0.09\,\mu b$	136	[23]
$\gamma p \to p\phi$	9.3	$0.55 \pm 0.07\,\mu b$	224	[23]
$\gamma p \to n a_2^+$	4.7–5.8	$1.7 \pm 0.9\,\mu b$		[25]
$\gamma p \to n a_2^+$	6.8–8.2	$0.9 \pm 0.9\,\mu b$		[25]
$\gamma p \to n a_2^+$	19.5	$0.29 \pm 0.06\,\mu b$	~ 100	[26]

Table 3.1: A sample of measured photoproduction cross sections from several references. Note the small numbers of events in any given channel.

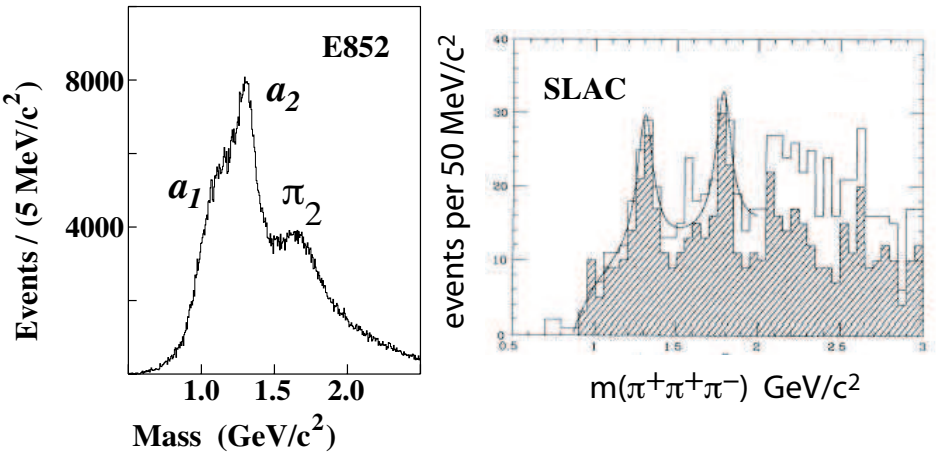

Figure 3.11: (left) The 3π mass spectrum from the reaction $\pi^- p \to \pi^+\pi^-\pi^- p$ at 18 GeV/c from E852 at Brookhaven. (right) The 3π mass spectrum from the reaction $\gamma p \to \pi^+\pi^+\pi^- n$ at 19 GeV from SLAC.

exotic $\pi_1(1600)$ in the published E852 results will be increased by four orders of magnitude by GLUEX after one year of running.

There are reasonable sized data sets in 2π and 2π photoproduction from the CLAS detector at JLab that are currently under analysis. However, these arise from unpolarized photon beams and are produced from an incoherent bremsstrahlung spectrum that peaks at around 5 GeV.

3.6 Complementarity with other searches

Gluonic excitations include both exotic and non-exotic hybrid mesons and glueballs. Hybrid mesons exist in both the light quark (u, d and s) and heavy quark (c and b) sectors. Clearly, existing data collected with incident π beams, central collisions, $\bar{p}p$ annihilations and e^+e^- collisions have not uncovered a wealth of information about these states. As discussed earlier, the focus of the GLUEX project is in the light-quark hybrid sector. The initial benchmark states will be the exotic hybrids, which cannot mix with $q\bar{q}$ and therefore have a *smoking gun* signature. There are good reasons to expect that photoproduction will be particularly effective at uncovering the exotic hybrid mesons. And the existing photoproduction data are meager indeed.

The glueball and heavy hybrid sectors are not accessible to GLUEX. Glueballs are not preferentially produced in photoproduction because they do not

couple to photons. Moreover, according to lattice QCD, the lightest exotic glueball has a mass of 4 GeV/c^2. One fruitful area of investigation are J/ψ radiative decays since the system recoiling from the photon should be rich in two-gluon states. The planned CLEO-c project at CESR will collect a billion J/ψ radiative decays.

The direct production of exotic hybrids in e^+e^- collisions is complicated by the fact that the angular momentum barrier (the excited flux-tube carries $J = 1$) suppresses this production mode.

Lattice QCD predictions about heavy-quark exotic hybrids are at as reliable as for the light-quark hybrids but the experimental situation is far more problematic. The photoproduction cross-sections are a few orders of magnitude lower. At the higher energies needed to produce these more massive states many other uninteresting processes can contribute to background. Finally, to unambiguously tag a charm or beauty hybrid one must identify detached vertices, further complicating the experimental challenge.

3.7 Production and analysis of hybrid mesons

3.7.1 Kinematics

Consider a specific exclusive photoproduction reaction:

$$\gamma p \to X p \tag{3.1}$$

The center-of-mass energy squared, s, and the momentum-transfer-squared, t, between the incoming beam and outgoing X are defined in terms of the four-vectors of the particles:

$$s = (p_\gamma + p_p)^2 \tag{3.2}$$

$$t = (p_\gamma - p_X)^2 \tag{3.3}$$

The dependence of the cross section on s and t depend on the production mechanism, which is usually described in terms of the particle or particles which can be exchanged as shown in Figure 3.12. For example, if the exchange particle is the pomeron (diffractive process) the cross section is nearly constant in s. For meson-exchange processes, cross sections typically fall off with increasing s. The dependence on t is typically exponential:

$$\frac{dN}{dt} \propto e^{-\alpha|t|} \tag{3.4}$$

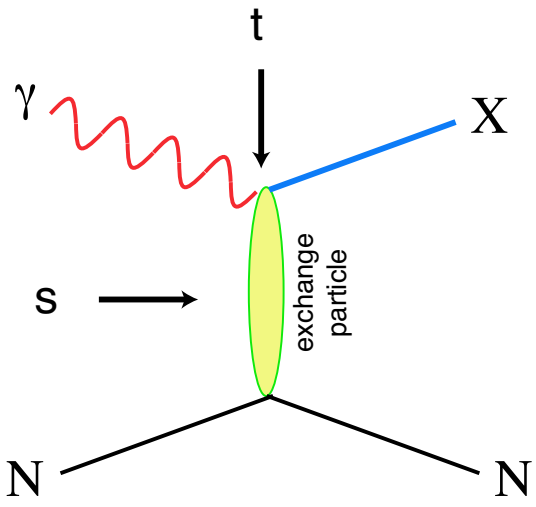

Figure 3.12: Diagram for the photoproduction of particle X. The variables s and t are the center-of-mass energy squared and the momentum-transfer-squared from incoming photon to outgoing particle X. The process shown here proceeds through the exchange of a particle in the t-channel.

For the process (3.1) at high enough photon beam energy, E_γ, we can make the approximation $s \approx 2 \cdot E_\gamma$ where E_γ is in GeV and s is in GeV^2. For fixed s and mass of X, m_X, there is a minimum value of $|t|$, or $|t|_{min}$, needed to produce X. This $|t|_{min}$ increases with increasing m_X for fixed E_γ and decreases with increasing E_γ for fixed m_X. Coupled with the steep dependence implied in equation (3.4), the dependence of $|t|_{min}$ on m_X will affect event yields. In addition, the line shape of a resonance can be distorted if there is too rapid a variation of $|t|_{min}$ across the width of a resonance.

Figure 3.13 shows an example of how the dependence in t is correlated with particle exchange. The distribution is in $|t'|$ where $t' = t - t_{min}$ for the D-waves after a PWA of the $\eta\pi^0$ system from the reaction $\pi^- p \to \eta\pi^0 n$ at 18 GeV/c. The curves are fits to expected Regge exchanges for the various D-waves.

3.7.2 PWA requirements

The PWA technique is described in a later chapter. It is important to stress here that the detector design focuses on hermeticity and resolution to insure nearly uniform coverage with well-understood acceptance functions for various decay angles for particle X. Kinematic fitting will also be used to identify

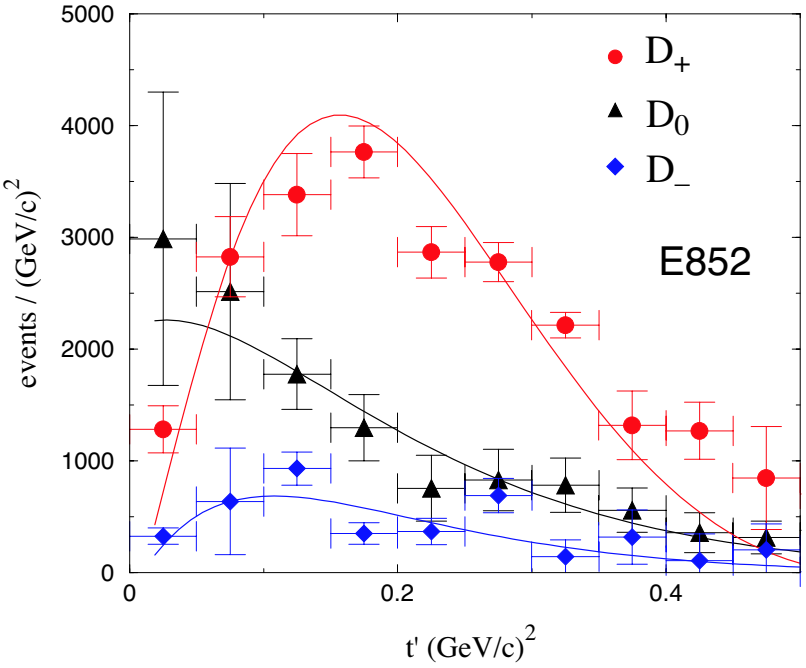

Figure 3.13: The distribution in $|t'|$ where $t' = t - t_{min}$ for the D-waves after a PWA of the $\eta\pi^0$ system from the reaction $\pi^- p \to \eta\pi^0 n$ at 18 GeV/c. The curves are fits to expected Regge exchanges for the various D-waves.

exclusive processes. The design focuses on the requirements of the PWA. The existence of well established resonances will be used as benchmarks for the PWA. They also provide benchmarks for the phase variation of candidate exotic states. Furthermore, candidate exotics can appear with multiple decay modes which should give consistent results. As an example, a meson which decays into $\eta\pi$ should be observed in channels where $\eta \to \pi^+\pi^-\pi^0$, $\eta \to 3\pi^0$, and $\eta \to 2\gamma$. Each of these modes leads to different acceptances and systematics. This provides a powerful check on PWA results.

3.7.3 Linear polarization of the beam

Linear and circular polarization

We start with a review of the relationship between linear and circular polarization. A right-handed-circularly ($|R\rangle$) polarized photon has $m = 1$ while for a $|L\rangle$ photon $m = -1$. These are related to the linear polarization states, $|x\rangle$ (in production plane) and $|y\rangle$ (perpendicular to production plane) by:

$$|x\rangle = \frac{1}{\sqrt{2}}\left(|L\rangle - |R\rangle\right) \tag{3.5}$$

$$|y\rangle = \frac{i}{\sqrt{2}}\left(|L\rangle + |R\rangle\right) \tag{3.6}$$

States of linear polarization are eigenstates of parity. We will use these relations in several straightforward cases to show how linear polarization:

1. can provide information on decays in lieu of statistics,
2. is essential in isolating production mechanisms, and
3. can be used as an exotics filter if the production mechanism is known.

Linear polarization and statistics

To illustrate how linear polarization provides useful information in the PWA, consider the case of the photoproduction of a vector meson which subsequently decays into two pseudoscalar mesons. Possible examples are $\rho \to \pi\pi$ or $\phi \to K\bar{K}$. Suppose the production mechanism produces the vector with the same helicity as the incident photon (or *s-channel helicity conservation*). In the rest frame of the vector the two-pseudoscalar wave function is described by

$$Y_1^m(\theta, \phi) \propto \sin\theta \cdot e^{im\phi} \tag{3.7}$$

For circularly polarized photons (either $m = 1$ or $m = -1$) the square of this amplitude carries no ϕ information while for in-plane photons there is a $\cos^2\phi$ dependence and out-of-plane a $\sin^2\phi$ dependence in the decay angular distribution, since in these cases we have the sum or difference of Y_1^{+1} and Y_1^{-1} according to equations (3.5) and (3.6). Although not essential in determining spin, a gain of statistics is needed to recover a drop in the degree of linear polarization. For example, our Monte Carlo simulation studies indicate that when the degree of linear polarization decreases from 0.40 to 0.2 a factor of two increase in statistics is needed to achieve the same relative error in determination of spin amplitudes.

Linear polarization and production mechanism

This is best illustrated by considering a specific example. Suppose we produce a vector particle ($J^P = 1^-$) by the exchange of a scalar particle ($J^P = 0^+$ – natural parity exchange) or a pseudoscalar particle ($J^P = 0^-$ – unnatural parity exchange). We wish to determine whether the vector is produced by natural (amplitude A_N) or unnatural (amplitude A_U) parity exchange. In the center-of-mass of the vector particle, the momentum vectors of the beam photon and exchange particle are collinear. For circularly polarized photons, the m of the vector is the same as that of the photon. From parity conservation, the orbital angular momentum between the photon and exchange particle is $L = 0$ or $L = 2$ for natural parity exchange and $L = 1$ for unnatural parity exchange. So for circularly polarized photons, with $m = +1$, the total amplitude is $A_N + A_U$ whereas for $m = -1$, the total amplitude is $A_N - A_U$. This follows simply from the addition of angular momenta. Circularly polarized photons allow us to measure only the sum or difference of the two exchange amplitudes. If however, we have linearly polarized photons along the x-direction, we extract A_N using equation (3.5) and for polarization along the y-direction, we extract A_U using equation (3.6).

Linear polarization as an exotics filter

Using arguments similar to those above, it has been shown [32] that linear polarization can be used as a tool to filter exotics. For example, a $\rho\pi$ system with $I = 1$ has $C = +$. Suppose that one can determine the naturality of the exchange particle by selecting data within a range of $|t|$. For a produced $C = +$ particle with spin one we can have natural parity ($J^{PC} = 1^{-+}$ – exotic) or unnatural parity ($J^{PC} = 1^{++}$ – non-exotic). In the case of natural parity exchange the in-plane polarization selects the $J^{PC} = 1^{-+}$ wave while out-

of-plane polarization selects $J^{PC} = 1^{++}$. For unnatural parity exchange the reverse is true. Note that in this case, we are specifying the naturality of the exchange and using linear polarization to select the naturality of the produced particle. In the previous section, we specified the naturality of the produced particle and used linear polarization to select the naturality of the exchanged particle.

Bibliography

[1] Y. Nambu. Univ. of Chicago report No. 70-70, 1970.

[2] C.Bernard *et al.* (MILC Collaboration). *Phys. Rev.*, D**56**:7039, 1997. hep-lat/9707008.

[3] N. Isgur, R. Kokoski, and J. Paton. *Phys. Rev. Lett.*, **54**:869, 1985.

[4] P.Lacock *et al.* (UKQCD Collaboration). *Phys. Lett.*, B**401**:308, 1997.

[5] N. Isgur and J. Paton. Flux-tube model for hadrons in QCD. *Phys. Rev.*, D**31**:2910, 1985.

[6] C.J. Morningstar and M. Peardon. Efficient glueball simulations on anisotropic lattices. *Phys. Rev.*, D**56**:4043, 1997.

[7] G.S. Bali *et al. Phys. Lett.*, B**309**:378, 1993.

[8] J.Sexton *et al.* (IBM Collaboration). *Phys. Rev. Lett.*, **75**:4563, 1995.

[9] G. Bali *et al.* (SESAM Collaboration). *Nucl. Phys. Proc. Suppl.*, **63**:209, 1998. hep-lat/9710012.

[10] C.Amsler and F.E.Close. *Phys. Lett.*, B**353**:385, 1995.

[11] C.Amsler and F.E.Close. Is the $f_0(1500)$ a scalar glueball? *Phys. Rev.*, D**53**:295, 1996.

[12] F. E. Close and A. Kirk. Scalar glueball-qqbar mixing above 1 gev and implications for lattice qcd. *Eur. Phys. J.*, C**21**:531–543, 2001. hep-ph/0004241.

[13] G. S. Adams *et al.* (E852 Collaboration). *Phys. Rev. Lett.*, **81**:5760, 1998.

[14] E.I. Ivanov *et al.* (E852 Collaboration). Observation of Exotic Meson Production in the Reaction $\pi^- p \to \eta' \pi - p$ at 18-GeV/c. *Phys. Rev. Lett.*, **86**:3977, 2001.

[15] D. R. Thompson *et al.* (E852 Collaboration). *Phys. Rev. Lett.*, **79**:1630, 1997.

[16] A.Abele *et al.* (Crystal Barrel Collaboration). Exotic $\pi\eta$ State in $\bar{p} - d$ Annihilation at Rest into $\pi^-\pi^0\eta p_{spectator}$. *Phys. Lett.*, B**423**:175, 1998.

[17] D. Alde *et al. Phys. Lett.*, B**205**:397, 1988.

[18] Yu. Prokoshkin, S. A. Sadovski. *Phys. Atom. Nucl.*, **58**:606, 1995.

[19] G. M. Beladidze *et. al. Phys. Lett.*, B**313**, 1993.

[20] H. Aoyagi *et. al. Phys. Lett.*, B**314**, 1993.

[21] A. Afanasev and P. R. Page. Photoproduction and Electroproduction of $J^{PC} = 1^{-+}$ exotics. *Phys. Rev.*, D**57**:6771, 1998.

[22] A. P. Szczepaniak and M. Swat. *Phys. Lett.*, B**516**:72, 2001.

[23] J. Ballam *et al.* Vector-meson production by polarized photons from 2.8, 4.7, and 9.3 GeV. *Phys. Rev.*, D**7**:3150–3177, 1973.

[24] K. Abe *et al. Phys. Rev. Lett.*, **53**:751, 1984.

[25] Y. Eisenberg *et al. Phys. Rev.*, D**5**:15, 1972.

[26] G. T. Condo, T. Handler, W. M. Bugg, G. R. Blackett, M. Pisharody and K. A. Danyo. Further results from charge-exchange photoproducton. *Phys. Rev.*, D**48**:3045, 1993.

[27] M. Atkinson *et al* (The Omega Collaboration). *Nucl. Phys.*, B**231**:15, 1984.

[28] M. Davier *et al.* The reaction $\gamma p \to \pi^+\pi^-\pi^+\pi^- p$ at high-energy and γ dissociation into 4π. *Nucl. Phys.*, B**58**:31, 1973.

[29] K. Abe *et al. Phys. Rev.*, D**32**:2288, 1985.

[30] M. Atkinson *et al* (The Omega Collaboration). *Nucl. Phys.*, B**243**:1, 1984.

[31] G. R. Blackett *et al.* The Photoproduction of the $b_1(1235)\pi$ System. Technical report, August 1997. hep-ex/9708032.

[32] A. V. Afanasev and A. P. Szczepaniak. Charge exchange $\rho^0\pi^+$ photoproduction and implications for searches for exotic mesons. *Phys. Rev. D*, **61**:114008, 2000.